University of Nebraska - Lincoln
DigitalCommons@University of Nebraska - Lincoln

Special Education and Communication Disorders Faculty Publications

Department of Special Education and Communication Disorders

2022

Dynamic causal modeling of neural responses to an orofacial pneumotactile velocity array

Yingying Wang
University of Nebraska-Lincoln, yingying.wang@unl.edu

Rebecca Custead
University of Nebraska-Lincoln

Hyuntaek Oh
University of Nebraska-Lincoln

Steven M. Barlow
University of Nebraska-Lincoln, steven.barlow@unl.edu

Follow this and additional works at: https://digitalcommons.unl.edu/specedfacpub

Part of the Special Education and Teaching Commons

Wang, Yingying; Custead, Rebecca; Oh, Hyuntaek; and Barlow, Steven M., "Dynamic causal modeling of neural responses to an orofacial pneumotactile velocity array" (2022). *Special Education and Communication Disorders Faculty Publications*. 239.
https://digitalcommons.unl.edu/specedfacpub/239

This Article is brought to you for free and open access by the Department of Special Education and Communication Disorders at DigitalCommons@University of Nebraska - Lincoln. It has been accepted for inclusion in Special Education and Communication Disorders Faculty Publications by an authorized administrator of DigitalCommons@University of Nebraska - Lincoln.

Neuroimage: Reports 2 (2022) 100081

Contents lists available at ScienceDirect

Neuroimage: Reports

journal homepage: www.sciencedirect.com/journal/neuroimage-reports

Dynamic causal modeling of neural responses to an orofacial pneumotactile velocity array

Yingying Wang [a,b,c,d,*], Rebecca Custead [e], Hyuntaek Oh [d,e], Steven M. Barlow [b,d,e]

[a] Neuroimaging for Language, Literacy and Learning Laboratory, Department of Special Education and Communication Disorders, University of Nebraska-Lincoln, Lincoln, NE, USA
[b] Center for Brain, Biology and Behavior, University of Nebraska-Lincoln, Lincoln, NE, USA
[c] Nebraska Center for Research on Children, Youth Families and Schools, University of Nebraska-Lincoln, Lincoln, NE, USA
[d] Department of Biological Systems Engineering, University of Nebraska-Lincoln, Lincoln, NE, USA
[e] Communication Neuroscience Laboratory, Department of Special Education and Communication Disorders, University of Nebraska-Lincoln, Lincoln, NE, USA

ARTICLE INFO

Keywords:
Dynamic causal modeling
Orofacial
Pneumotactile stimulation
fMRI
Saltatory velocity
Effective connectivity

ABSTRACT

The effective connectivity of neuronal networks during orofacial pneumotactile stimulation with different velocities is still unknown. The present study aims to characterize the effectivity connectivity elicited by three different saltatory velocities (5, 25, and 65 cm/s) over the lower face using dynamic causal modeling on functional magnetic resonance imaging data of twenty neurotypical adults. Our results revealed the contralateral SI and SII as the most likely sources of the driving inputs within the sensorimotor network for the pneumotactile stimuli, suggesting parallel processing of the orofacial pneumotactile stimuli. The 25 cm/s pneumotactile stimuli modulated forward interhemispheric connection from the contralateral SII to the ipsilateral SII, suggesting a serial interhemispheric connection between the bilateral SII. Moreover, the velocity pneumotactile stimuli influenced the contralateral M1 through contralateral SI and SII, indicating that passive pneumotactile stimulation may positively impact motor function rehabilitation. Furthermore, the medium velocity 25 cm/s pneumotactile stimuli modulated both forward and backward connections between the right cerebellar lobule VI and the contralateral left SI and M1. This result suggests that the right cerebellar lobule VI plays a role in the sensorimotor network through feedforward and feedback neuronal pathways. This study is the first to map similarities and differences of effective connectivity across the three-velocity orofacial pneumotactile stimulation. Our findings shed light on the potential therapeutic use of passive orofacial pneumotactile stimuli using the Galileo system.

1. Introduction

Functional brain imaging studies have provided insights into the human sensorimotor networks. The primary (SI) and secondary (SII) somatosensory cortices, and the primary motor cortex (M1) are the core brain regions within the sensorimotor networks (Ackerley et al., 2012; Custead et al., 2017; Grodd et al., 2001; Oh et al., 2017). The contralateral SI and bilateral SII have been activated during various types of touch (Ackerley et al., 2012; Disbrow et al., 2001; Francis et al., 2000; Ionta et al., 2014; Ruben et al., 2001). The contralateral M1 has been involved during passive touch or air pressure pule stimulation to the hands' glabrous skin (Ackerley et al., 2012; Francis et al., 2000; Oh et al., 2017). For the face, there is scanty evidence on how moving tactile stimulation is processed in the brain. Additionally, the functional representations of moving tactile stimulation have primarily used electric stimulation or passive touch on the glabrous hand (Ackerley et al., 2012; Lin and Kajola, 2003; Oh et al., 2017). Our previous study is the first to use air-pulsed pneumotactile stimuli on the right lower face to elicit a bilateral SI, left M1, and the right lobule VI (Custead et al., 2017). A subsequent functional connectivity (FC) analysis on the same data revealed that the medium velocity (25 cm/s) tactile stimulation evoked stronger FC in the ipsilateral cortical regions than the low velocity (5 cm/s) (Wang et al., 2020). Nevertheless, there is still much to learn about the complex neuronal networks involved in orofacial pneumotactile velocity processing. Gaining more insights into the human sensorimotor networks may stimulate the development of innovative

* Corresponding author. Neuroimaging for Language, Literacy and Learning laboratory, Department of Special Education and Communication Disorders, University of Nebraska-Lincoln, Lincoln, NE, USA.
E-mail address: yingying.wang@unl.edu (Y. Wang).

https://doi.org/10.1016/j.ynirp.2022.100081
Received 17 July 2021; Received in revised form 29 December 2021; Accepted 10 January 2022
Available online 16 January 2022
2666-9560/© 2022 The Authors. Published by Elsevier Inc. This is an open access article under the CC BY-NC-ND license (http://creativecommons.org/licenses/by-nc-nd/4.0/).

neurotherapeutic programs for patients with brain injuries (i.e., stroke, traumatic brain injury, etc.) to improve their rehabilitation outcomes (i.e., motor skills in the hand or foot, orofacial systems for speech and swallowing).

The serial processing theory suggests that somatosensory stimulation flows predominantly from the contralateral thalamus to the contralateral SI and then to the contralateral SII. The contralateral SI receives the driving inputs from tactile stimuli and initiates the higher-order processing of the spatiotemporal information about the tactile stimuli (Disbrow et al., 2001; Lundblad et al., 2011; Norrsell and Olausson, 1994). Animal studies using electrophysiological and anatomical tracing approaches found extensive cortico-cortical projections between SI and SII (Burton and Carlson, 1986; Friedman et al., 1980; Pons and Kaas, 1986). In humans, a small number of studies using dynamic causal modeling (DCM) with functional magnetic resonance imaging (fMRI) data have suggested that both innocuous and noxious tactile stimuli are processed in serial mode (from SI to SII) (Kalberlah et al., 2013; Khoshnejad et al., 2014). In contrast, the parallel processing theory proposes that somatosensory stimulation is directly transmitted to both contralateral SI and SII. Animal studies have reported that direct thalamocortical inputs to SII bypassing SI (Rowe et al., 1996; Turman et al., 1992; Zhang et al., 1996, 2001) and direct projections from thalamic nuclei (i.e., the ventral posterior nucleus, the ventral posterior inferior nucleus, etc.) to both SI and SII (Jones, 1998; Krubitzer and Kaas, 1992). Several human studies also supported the parallel processing theory using various imaging approaches (Klingner et al., 2015; Liang et al., 2011; Raij et al., 2008; Song et al., 2021). A multimodal imaging study suggested that parallel inputs to both SI and SII facilitate long-distance cortico-cortical connections using magnetoencephalography (MEG) and single-pulse transcranial magnetic stimulation (TMS) with electroencephalography (EEG) during electrical stimuli to the dominant hand's median nerve (Raij et al., 2008). Liang et al. (2011) identified that the neural activities elicited by both innocuous and noxious tactile stimuli are best explained by DCM models where the fMRI responses in both SI and SII depend on direct inputs from the thalamus. Moreover, DCM studies of both MEG and fMRI data supported the parallel processing theory for both nociceptive and tactile information processing (Klingner et al., 2015; Song et al., 2021). In contrast, another DCM study of fMRI data revealed the coexistence of the serial and parallel modes between SI and SII during pressure stimulation (Chung et al., 2014). Taken together, whether tactile stimuli are processed in serial or parallel mode or both modes in humans remains unclear. Therefore, the present study will examine how orofacial pneumotactile stimuli are processed and whether the neuronal mechanism of tactile processing depends on different velocity tactile inputs.

The bilateral activation of SII elicited by unilateral somatosensory stimuli (Custead et al., 2017; Forss et al., 1994; Hari et al., 1993; Hoechstetter et al., 2001) and the existence of dense transcallosal fibers connecting the contralateral and ipsilateral SII (Jones and Powell, 1969b; Pandya and Vignolo, 1968; Picard et al., 1990) suggest that there are interhemispheric connections between the bilateral SII. In addition, the size of the corpus callosum was positively correlated with the peak amplitude of the ipsilateral SII during innocuous electrical stimuli to the right index finger (Stancak et al., 2002). Patients with callosotomy failed to show ipsilateral SII activation during unilateral tactile stimulation (Fabri et al., 1999). Therefore, both structural and functional interhemispheric connections exist between the bilateral SII. The present study will identify how pneumotactile information flows from the contralateral SII to the ipsilateral SII (i.e., via forward, backward, or both connections) in neurotypical adults. Our findings will provide important evidence on interhemispheric connections between bilateral SII during passive pneumotactile stimulation on the right lower face in 20 neurotypical adults. Research work has shown that brain injury caused by stroke or traumatic brain injury can induce interhemispheric changes resulting in changes in brain activity in the affected hemisphere via transcallosal inhibition and unaffected hemisphere via transcallosal disinhibition (Bannister et al., 2015; Cramer and Crafton, 2006; Mohajerani et al., 2011; Murase et al., 2004; Pellegrino et al., 2012). Functional connectivity studies also demonstrated that resting-state interhemispheric functional connectivity was associated with stroke recovery (Carter et al., 2010; Compston, 2011). Therefore, the interhemispheric connectivity may help evaluate functional brain reorganization after brain injury.

The cross-modality plasticity theory suggested that passive somatosensory stimuli could elicit neuronal responses to improve motor function (Ladda et al., 2014; Nasir et al., 2013; Pearson, 2000; Sanes and Donoghue, 2000). The face sensorimotor networks are essential for speech production, sucking, and swallowing. In addition, the integration of sensory and motor functions is critical for motor control and learning (Barlow and Estep, 2006; Barlow and Stumm, 2010; Sessle et al., 2005, 2007; Smith, 2016). To date, little is known about how orofacial pneumotactile stimuli propagate through the sensorimotor networks. Moreover, passive motor and sensory stimulations of hands and feet have elicited equal activation levels in the sensorimotor cortex as the active motor tasks (Blatow et al., 2011). High-frequency passive repetitive sensory stimulation, utilizing Hebbian learning principles, has been successfully used to treat chronic stroke patients and improve their sensorimotor functions without the need for active participation (Ahn et al., 2016b; Chen et al., 2018b; Conforto et al., 2007; Powell et al., 1999; Smith et al., 2009). The present study aims to determine whether passive orofacial pneumotactile stimulation can effectively elicit brain activity in M1. If so, functional changes in M1 may positively impact motor function. Thus, our findings of the effective connectivity within the sensory and motor system revealed by DCM in this study will elucidate the neural pathways supporting sensory-motor integration and the neural mechanism underlying how passive orofacial pneumotactile stimuli are processed in neurotypical adults. This study will uncover the impact of passive somatosensory stimulation on the primary motor cortex and shed light on the development of innovative neurotherapeutic rehabilitation programs. Patients who are unable to perform active movements right after brain injury (e.g., due to stroke, traumatic brain injury, etc.) may benefit from early interventions with passive sensory and motor stimulations.

The cerebellum is recognized to be involved mostly in motor control and motor learning (Albus, 1971; Marr, 1969), but growing evidence has suggested its role in the processing of cognition and emotion (Buckner, 2013; D'Angelo and Casali, 2012; Schmahmann and Caplan, 2006). Through the cerebellar peduncles, all cerebellar nuclei are interconnected with the rest of the brain. The dentate nucleus, connected to thalamic nuclei and sensorimotor regions through the superior peduncle (Dum and Strick, 2003; Tellmann et al., 2015), has been involved in speech or cognitive learning (Thurling et al., 2011). Recent evidence has also supported that the cerebellum can be subdivided into several specialized functional regions (Witter and De Zeeuw, 2015). Our previous work has demonstrated that the right lobule VI was a part of the sensorimotor somatotopic representations for the face (Custead et al., 2017; Grodd et al., 2001; Wang et al., 2020). The effective connectivity of the cortico-cerebral networks elicited by passive orofacial pneumotactile stimulation has not yet been studied, which will provide unique insights into the feedforward and feedback pathways of tactile processing in the cortico-cerebral networks.

Our previous study identified similarities and differences of functional connectivity in the sensorimotor system during orofacial pneumotactile stimuli of different velocities (5, 25, 65 cm/s) and shed light on the functional networks encoding the orofacial pneumotactile perception of velocity (Wang et al., 2020). However, the functional connectivity is limited to undirected connections among regions, and the causal relationships within the sensorimotor network cannot be examined. The directed causal influences among neural populations are defined as effective connectivity. In fMRI-based causality analysis, DCM is the predominant analysis framework for characterizing effective connectivity within distributed neuronal responses (Friston et al., 2019;

Zeidman et al., 2019a, 2019b). Granger Causality (GC) is another representative approach that uses autoregressive models for causality analysis (Friston, 2011). GC measures lagged functional connectivity rather than strictly effective connectivity. Additionally, many assumptions of GC are violated in fMRI data based on simulated fMRI data (Smith et al., 2011). Unlike GC, DCM examines the instantaneous rates of changes in neural activity in response to experimental conditions, which is more suited to task-based fMRI analyses (Friston, 2011). The principle of DCM is that neural activity propagates through brain networks as in an input-state-output system, where causal interactions are mediated by hidden neuronal dynamics (Friston et al., 2013). Classical deterministic bilinear DCM uses a bilinear state equation with three components, including experimental (driving) inputs perturbing brain states (i.e., in our case, different velocity tactile stimuli), intrinsic connectivity in the absence of experimental perturbations, and modulations of the intrinsic connectivity induced by experimentally manipulated inputs (i.e., changes in regional couplings by tactile stimuli), which provided information concerning how much activation in source regions receiving direct inputs caused an increase/decrease in activation in target regions per unit of time. Unlike GC, DCM for fMRI does not account for conduction delays in the time series, which is not necessary because of the larger regional variability in hemodynamic response latencies resulting in limited temporal information. The inter-regional axonal conduction delay is typically in the order of 10–20 ms (Friston et al., 2003). The default bilinear model in SPM12 is chosen because the modulatory effects from the passive orofacial pneumotactile stimuli are the interaction between the neural activity and experimental inputs (switching the input-state-output brain system on and off) (Stephan et al., 2010). Therefore, DCM is well suited to examine the directed causal relationships within the sensorimotor network during passive orofacial pneumotactile stimulation in this study.

The present study aimed to identify effective connectivity in 20 neurotypical adults' fMRI data using DCM during orofacial pneumotactile stimuli through a 5-channel array at three saltatory velocities (5, 25, and 65 cm/s). This work is an extension of our previous studies (Custead et al., 2017; Wang et al., 2020) and will provide new information on the causal relationships between brain regions within the sensorimotor systems responsible for encoding the velocity tactile stimulation. We aimed to address the following questions on 1) whether orofacial pneumotactile stimuli (5, 25, and 65 cm/s) are processed serially from the contralateral SI to the contralateral SII or parallelly to both contralateral SI and SII, 2) how orofacial pneumotactile stimuli (5, 25, and 65 cm/s) influence interhemispheric connections between the contralateral SII and the ipsilateral SII, 3) how passive orofacial pneumotactile stimuli (5, 25, and 65 cm/s) influence the contralateral M1, and 4) what is the role of the right lobule VI in the sensorimotor networks during orofacial pneumotactile stimuli (5, 25, and 65 cm/s). Our results will provide direct evidence that passive orofacial pneumotactile stimuli with different velocities can induce functional changes in the sensorimotor network resulting in enhanced sensorimotor abilities after brain injury.

2. Methods

This study used a dataset that has been described in previous publications (Custead et al., 2017; Wang et al., 2020), which provides additional details regarding participants, paradigms, and fMRI data preprocessing.

2.1. Participants

Twenty healthy adults (mean age of 22.3, 15 females) were all right-handed, native English speakers and signed written informed consent forms to be enrolled in this study. They reported no history of neurological or psychiatric disorders. The present study was approved by the Institutional Review Board at the University of Nebraska–Lincoln (UNL).

2.2. Paradigms

The block-design fMRI paradigm presented each condition in a block of a 20-s task period followed by a 20-s rest period (Custead et al., 2017; Wang et al., 2020). The five task conditions consisting of 5 cm/s, 25 cm/s, 65 cm/s, "All on," and "All off" were randomly presented. The different velocities represented the different saltation speeds of the 60-ms air pressure pulses through the facial array. During the task condition, the participant passively received pneumotactile stimuli to the right facial skin by the Galileo Somatosensory™ system (a multichannel pneumatic amplifier and tactile array, Epic Medical Concepts & Innovations, Inc., Mission, Kansas, K.S., U.S.A.). During the rest condition, a visual countdown on the screen was used to maintain the participant's vigilance using E-Prime 2.0 (Psychology Software Tools, Pittsburgh, P.A., U.S.A.). Participants were instructed to pay attention to the number shown on the screen for 0.5 s to minimize brain activation in the primary visual cortex. A declining numeric countdown from 20 to 1 was used to indicate the rest period's remaining time. To reduce the effect of fatigue, we did three runs separately and offered optional breaks between runs. Each run consisted of 20 blocks, including four blocks of 5 cm/s, four blocks of 25 cm/s, four blocks of 65 cm/s, four blocks of "All on," and four blocks of "All off" (Custead et al., 2017; Wang et al., 2020). In total, each condition block lasted 960 s with a 480-s condition segment and a 480-s rest segment. Nineteen participants completed all three runs, and one participant completed two runs.

2.3. Image acquisition

All images were collected using a 3T Siemens Skyra MRI system (Siemens Medical Solutions, Erlangen, Germany) with a 32-channel head coil at the Center for Brain, Biology and Behavior at UNL. A high-resolution T1-weighted three-dimensional anatomical scan was acquired using magnetization-prepared rapid gradient-echo sequences (MPRAGE) with the following parameters: TR/TE/TA = 2.4 s/3.37 ms/5:35 min, flip angle = 7°, field of view = 256 × 256 mm, spatial resolution = 1 × 1 × 1 mm^3, number of slices = 192. Following the anatomical scan, the functional MRI (fMRI) scans were recorded using a T2*-weighted echo-planar imaging (EPI) sequence with the following parameters: TR/TE/TA = 2.5 s/30 ms/800 s, voxel size = 2.5 × 2.5 × 2.5 mm^3, flip angle = 83°, number of slices = 41, number of volumes = 320.

2.4. Preprocessing and general linear model

All image data from each run were preprocessed using the SPM12 toolbox (Wellcome Department of Imaging Neuroscience, University College London, U.K.), including motion correction through spatial realignment, structural segmentation and normalization, coregistration between functional scans and anatomical scan, and smoothing with 8 mm full-width at half-maximum (FWHM) using a Gaussian Kernel. The time series from each ROIs were concatenated for DCM analysis.

At the first (individual) level, the general linear model (GLM) estimated the parameters for each task condition when controlling motion using six rigid-body parameters as nuisance regressors. The overall main effect of velocity (5, 25, 65 cm/s) was computed with *F*-test using analysis of variance (ANOVA). Three *T*-test contrasts included 5 cm/s > rest, 25 cm/s > rest, 65 cm/s > rest. At the second (group) level, individual SPM results were pooled together for each contrast using a random-effect one-sample *T*-test. The bspmview toolbox (https://www.bobspunt.com/software/bspmview/) was used to create an axial view of slice montage. ($q < 0.05$, False discovery rate (FDR) corrected) (Benjamini and Hochberg, 1995).

2.5. Regions of interest and time-series extraction

The regions of interest (ROIs) were selected based on the group

results for each velocity stimulus. For 5 cm/s and 25 cm/s, ROIs included bilateral primary and secondary somatosensory cortices (left SI–LSI, SII–LSII, right SI–RSI, SII–RSII), left primary motor cortex (LM1), and right cerebellar lobule VI (RVI). For 65 cm/s, ROIs included the left primary and secondary somatosensory cortices. The coordinates of each ROI from the group results were used as the center of 8 mm radius spherical volumes to search a local maximum for each individual. Contrasts for the effect of each condition (5, 25, 65 cm/s) were used to identify peak voxels. Not all participants had significantly active voxels within each ROI. For each contrast of interest, mean-corrected (by an F-contrast for the effects of velocity) time series from each participant were extracted within 8 mm radius spherical volumes centered on each ROI using the first eigenvariate of voxels above a threshold of $p < 0.001$ (uncorrected).

2.6. Dynamic causal modeling

DCM was used in the present study to test hypotheses about the neuronal mechanisms that underlie experimental measurements of brain responses (Stephan et al., 2010). DCM uses bilinear differential equations with three components, including experimental (driving) inputs perturbing brain states (i.e., for our study, different velocity tactile stimuli elicit the cortex) (DCM.C matrix), intrinsic connectivity in the absence of experimental perturbations (DCM.A matrix), and changes (modulations) of the intrinsic connectivity induced by experimentally manipulated inputs (i.e., for our study, changes in regional couplings by tactile stimuli, which provided information concerning how much activation in source regions receiving direct inputs caused an increase/decrease in activation in target regions per unit of time) (DCM.B matrix) (Stephan et al., 2007). DCM can infer causal mechanisms in the brain networks and how external stimuli can change the causal relationships in the networks (Stephan et al., 2007, 2010). The model space in DCM analysis is constructed by hypotheses about the effective connectivity in the brain networks of interest.

To test whether pneumotactile saltatory stimuli to the right facial skin are processed using serial mode or parallel mode for each velocity, we constructed a set of six models for 5 and 25 cm/s and a set of two models for 65 cm/s (see Fig. 1). We included the intrinsic reciprocal connectivity (all forward and backward fixed connections) between the ROIs for each task condition. The pneumotactile stimuli were the driving inputs perturbing brain states either through the left SI only or both left SI and SII. To test whether velocity encoding modulates interhemispheric connection between the contralateral left SII and the ipsilateral right SII in forward-only mode, backward-only mode, or both forward and backward modes for 5 and 25 cm/s. We also included modulations of the intrinsic connectivity induced by either 5 or 25 cm/s stimuli. To examine how different velocities modulate the intrinsic connections between the left SI, SII, and M1, we constructed a set of three models for 5 and 25 cm/s (see Fig. 2), including modulating through forward connection from the left SI to left M1, or from the left SII to left M1, or from both the left SI and SII to left M1. To examine the cerebellum's role in somatosensory networks, we constructed a set of nine models, including the intrinsic reciprocal connectivity between the ROIs for 5 and 25 cm/s (see Fig. 3). The external velocity stimuli modulate the right cerebellar lobule VI through forward, or backward, or both connections to other ROIs (the left SI, SII, and M1).

2.7. Bayesian model selection and inference on parameters

The Bayesian model selection (BMS) compares each model's log evidence approximated using the free energy to select the winning model that explains the data as accurately as possible and has minimal complexity (Stephan et al., 2007, 2010). The model with the highest posterior probability is also the model with the most substantial evidence (Kass and Raftery, 1995; Rosa et al., 2012). Bayes factors have been used to compare two models (Kass and Raftery, 1995). Under the

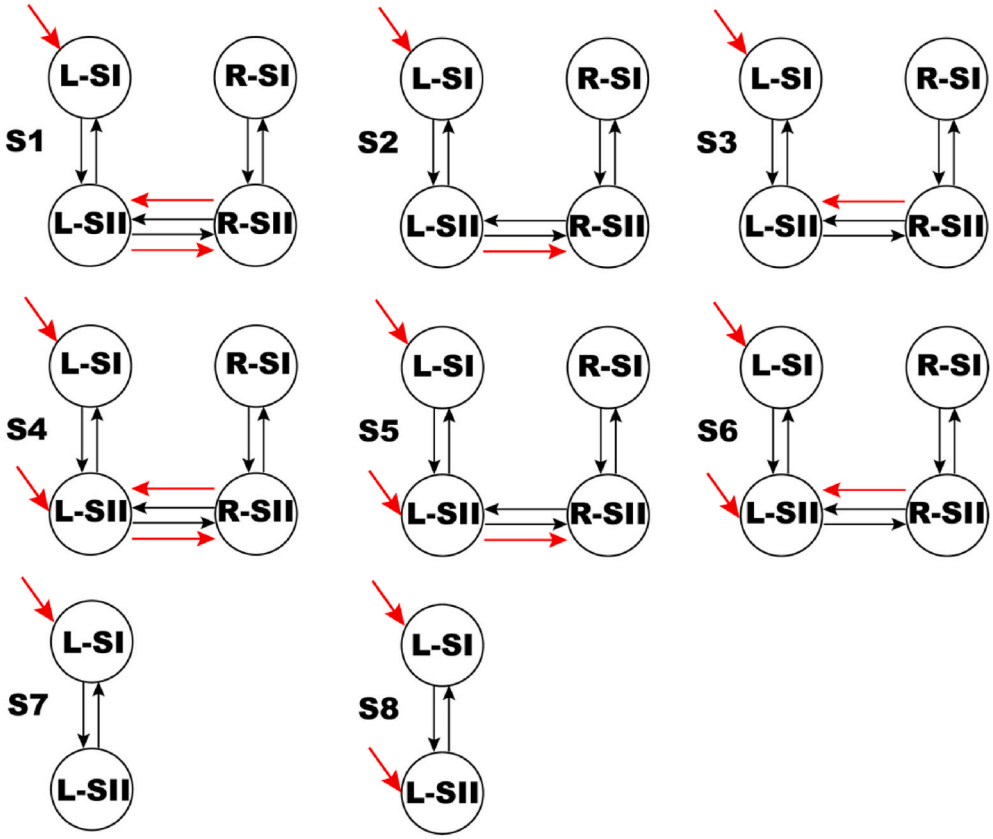

Fig. 1. L-SI: left primary somatosensory cortex, L-SII: left secondary somatosensory cortex, R–SI: right primary somatosensory cortex, R–SII: right secondary somatosensory cortex. Black arrows represent the intrinsic connections, Red arrows represent the modulatory connectivity and driving inputs to L-SI and L-SII. Models S1–S6 were examined for 5 and 25 cm/s. Models S7–S8 were examined for 65 cm/s. (For interpretation of the references to colour in this figure legend, the reader is referred to the Web version of this article.)

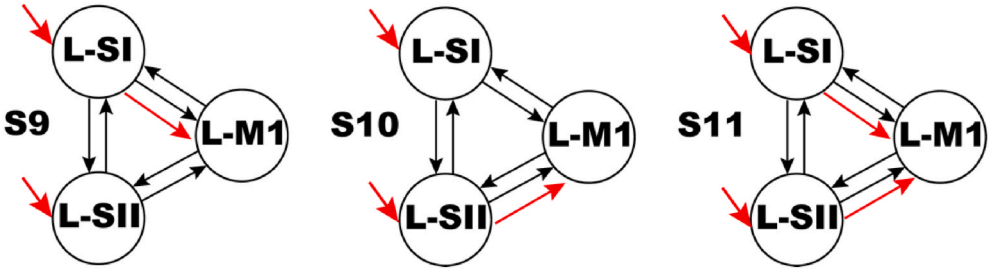

Fig. 2. L-SI: left primary somatosensory cortex, L-SII: left secondary somatosensory cortex, R–SI: right primary somatosensory cortex, R–SII: right secondary somatosensory cortex, L-M1: left primary motor cortex. Black arrows represent the intrinsic connections, Red arrows represent the modulatory connectivity and driving inputs to L-SI and L-SII. Models S9–S11 were examined for 5 and 25 cm/s. (For interpretation of the references to colour in this figure legend, the reader is referred to the Web version of this article.)

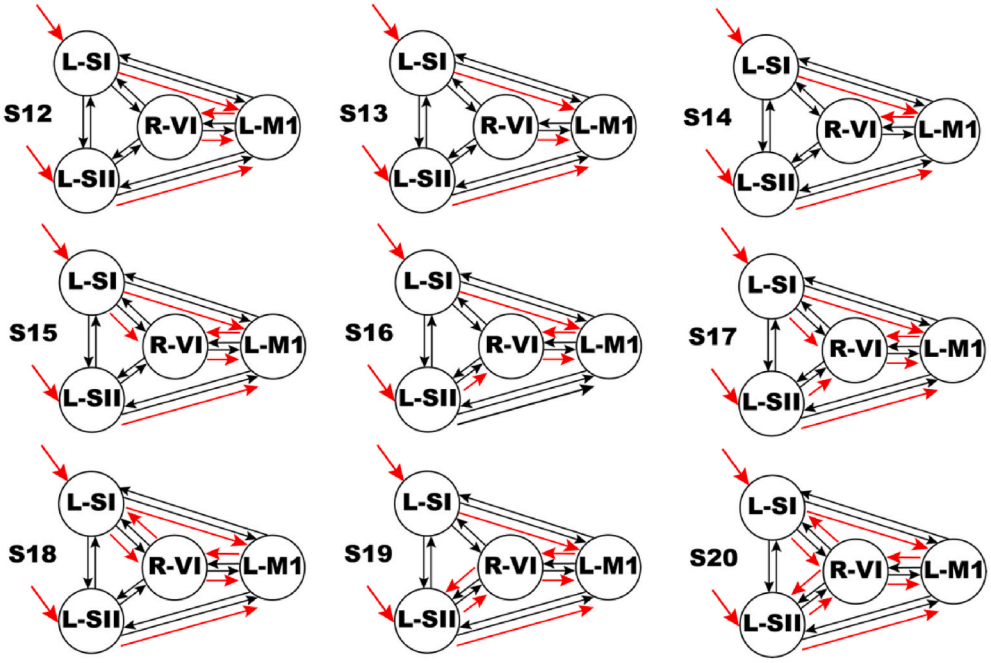

Fig. 3. L-SI: left primary somatosensory cortex, L-SII: left secondary somatosensory cortex, R–SI: right primary somatosensory cortex, R–SII: right secondary somatosensory cortex, L-M1: left primary motor cortex, R–VI: right cerebellar lobule VI. Black arrows represent the intrinsic connections, Red arrows represent the modulatory connectivity and driving inputs to L-SI and L-SII. Models S12–S20 were examined for 5 and 25 cm/s. (For interpretation of the references to colour in this figure legend, the reader is referred to the Web version of this article.)

uniform priors and Bayes' rule, a posterior model probability greater than 95% is equivalent to a Bayes factor greater than 20, which provides strong evidence in favor of one model over the other (Kass and Raftery, 1995; Rosa et al., 2012). A Bayes factor of 1–3 corresponding to a posterior model probability of 50–75% indicates weak evidence. A Bayes factor of 3–20 corresponding to a posterior model probability of 75–95% suggests positive evidence. We used a random-effects (RFX) approach for model selection at the group level, which allows each participant to have a different best model and computes the probability of all participants' data given each model. The model with high exceedance probability (EP) is the winning model. For the winning model, we considered the winning model's parameters as random effects in the population (i.e., velocity stimuli induced changes in connection strengths) (Stephan et al., 2010). Thus, the Bayesian model averaging (BMA) approach was used to compute the weighted averages of each model parameter. The weighting is determined by the posterior probability of each model (Stephan et al., 2010). Furthermore, the BMA values of the winning model were reported for each DCM analysis. We marked the connectivity parameters with the probability that the posterior estimate of the parameter is not zero greater than 85%. In addition, the modulation effects of velocity stimuli were compared using BMA results with one-sample paired *t*-tests with FDR correction for multiple comparisons (Benjamini and Hochberg, 1995) ($q < 0.05$, FDR corrected).

3. Results

3.1. GLM random-effects analysis

The group results were shown in Fig. 4, as identified in our previous report of this dataset (Custead et al., 2017; Wang et al., 2020). In the current DCM analysis, we focused on six ROIs for 5 and 25 cm/s and two ROIs for 65 cm/s. The group averaged coordinates were reported in Table 1.

3.2. DCM model comparison and selection

3.2.1. Driving inputs and interhemispheric connections

For both 5 and 25 cm/s, the winning model was S5 with the highest exceedance probability (5 cm/s: 85%, 25 cm/s: 51%) (Fig. 5). Somatosensory stimuli were driving inputs to both left SI and SII, and sensory stimuli only modulated the forward connection from contralateral left SII to the ipsilateral right SII. Based on Bayes' rule, there was strong evidence that the driving inputs entered the sensorimotor network through both left SI and SII for 5 cm/s (i.e., an exceedance probability of 85% relative to 0.7% for the best model among S1 to S3 with the driving inputs to the left SI only). For 25 cm/s, S5 with the highest exceedance probability (51%) is the winning model. However, there was weak evidence in favor of S5 over S3 (27%) since the Bayes factor was 1.5 computed by the ratio of model posterior means (0.3/0.2 = 1.5). For 65 cm/s, the winning model was S8 with the highest exceedance

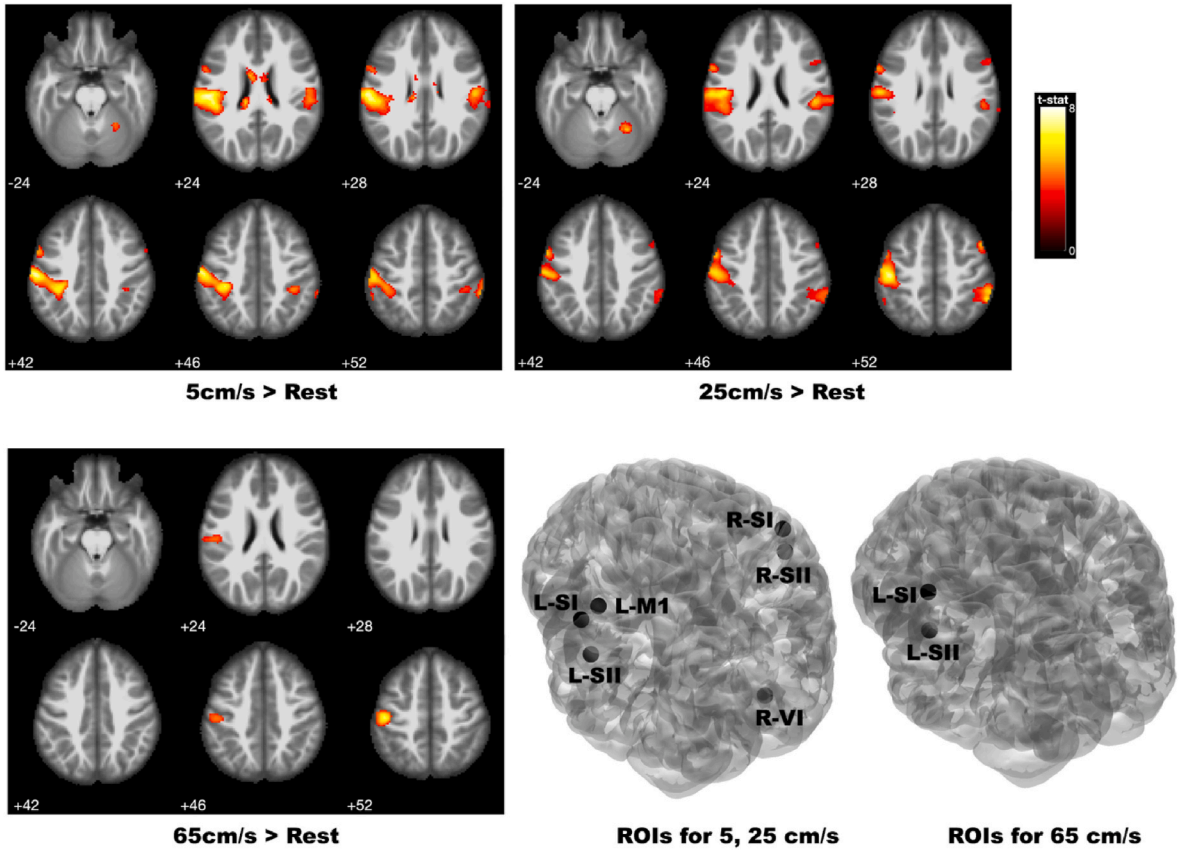

Fig. 4. Group results for 5 cm/s > Rest, 25 cm/s > Rest, 65 cm/s > Rest. ROIs for 5, 25, 65 cm/s. L-SI: left primary somatosensory cortex, L-SII: left secondary somatosensory cortex, R–SI: right primary somatosensory cortex, R–SII: right secondary somatosensory cortex, L-M1: left primary motor cortex, R–VI: right cerebellar lobule VI. Images are in neurological view: the left side of the image corresponds to the left side of the brain, and the right side of the image corresponds to the right side of the brain.

Table 1
Group averaged coordinates of ROIs' center in MNI space.

ROI	5 cm/s			25 cm/s			65 cm/s		
	X, Y, Z	N	T	X, Y, Z	N	T	X, Y, Z	N	T
Left SI	−56, −22, 45	19	6.3	−51, −20, 45	20	7.8	−53, −21, 50	17	7.8
Left SII	−54, −28, 24	17	5.7	−54, −25, 23	19	5.4	−53, −22, 26	15	4.5
Right SI	58, −18, 42	13	3.8	58, −15, 37	13	3.4			
Right SII	58, −20, 27	13	4.0	56, −22, 24	13	4.0			
Left M1	−47, −23, 51	17	3.6	−46, −23, 52	17	4.3			
Right VI	26, −57, −24	7	3.6	26, −56, −23	5	3.4			

N: the number of participants who had significantly active voxels within the ROI, T: averaged T-values, SI: primary somatosensory cortex, SII: secondary somatosensory cortex, M1: primary motor cortex. Right VI: Right cerebellar lobule VI.

probability (55%) (Fig. 5). A Bayes factor of 1 suggested that there was weak evidence in favor of S8 over S7 (45%). The driving inputs to both contralateral left SI and SII provided strong evidence on a parallel mode of processing for 5 cm/s and weak evidence on a parallel mode of processing for 25 and 65 cm/s. In addition, the 5 and 25 cm/s velocity stimuli both modulated the inter-hemispheric connection through the forward connection from the contralateral left SII to the ipsilateral right SII.

3.2.2. *Cross-modality plasticity*

For 5 cm/s, the S10 model has the highest exceedance probability of 50% (Fig. 6). The 5 cm/s velocity stimuli modulated only forward connection from the left SII to the left M1. However, there was weak evidence in favor of S10 over S11 (49%) since the Bayes factor was one, computed by the ratio of model posterior means (0.4/0.4 = 1). For 25 cm/s, the S11 model has the highest exceedance probability of 34% (Fig. 6). The 25 cm/s velocity stimuli modulated both forward connections from the left SI to the left M1 and the left SII to the left M1. But there was weak evidence in favor of S11 over S9 (Bayes factor = 1) or S10 (Bayes factor = 1). For 5 and 25 cm/s, S10 and S11 are the winning models over the S9 model.

3.2.3. *Feedforward and feedback loops of cortico-cerebral networks*

For 5 cm/s, S20 has the highest exceedance probability of 36% (Fig. 7). Only direct inputs to both L-SI and L-SII reached significance for the 5 cm/s velocity stimuli. The forward and backward connections between the right VI to the left SI, SII, and M1 failed to reach significance. There was weak evidence in favor of S20 over the second-best model S18 with the exceedance probability of 21% since the Bayes factor was 1.3. For 25 cm/s, S18 has the highest exceedance probability of 41% (Fig. 7). The forward and backward intrinsic connections between the right VI to the left SI and M1 were significant. There was weak evidence in favor of S18 over the second-best model S18 with the exceedance probability of 18% since the Bayes factor was 1.5. For 5 and 25 cm/s, S18 and S20 are the winning models over other models.

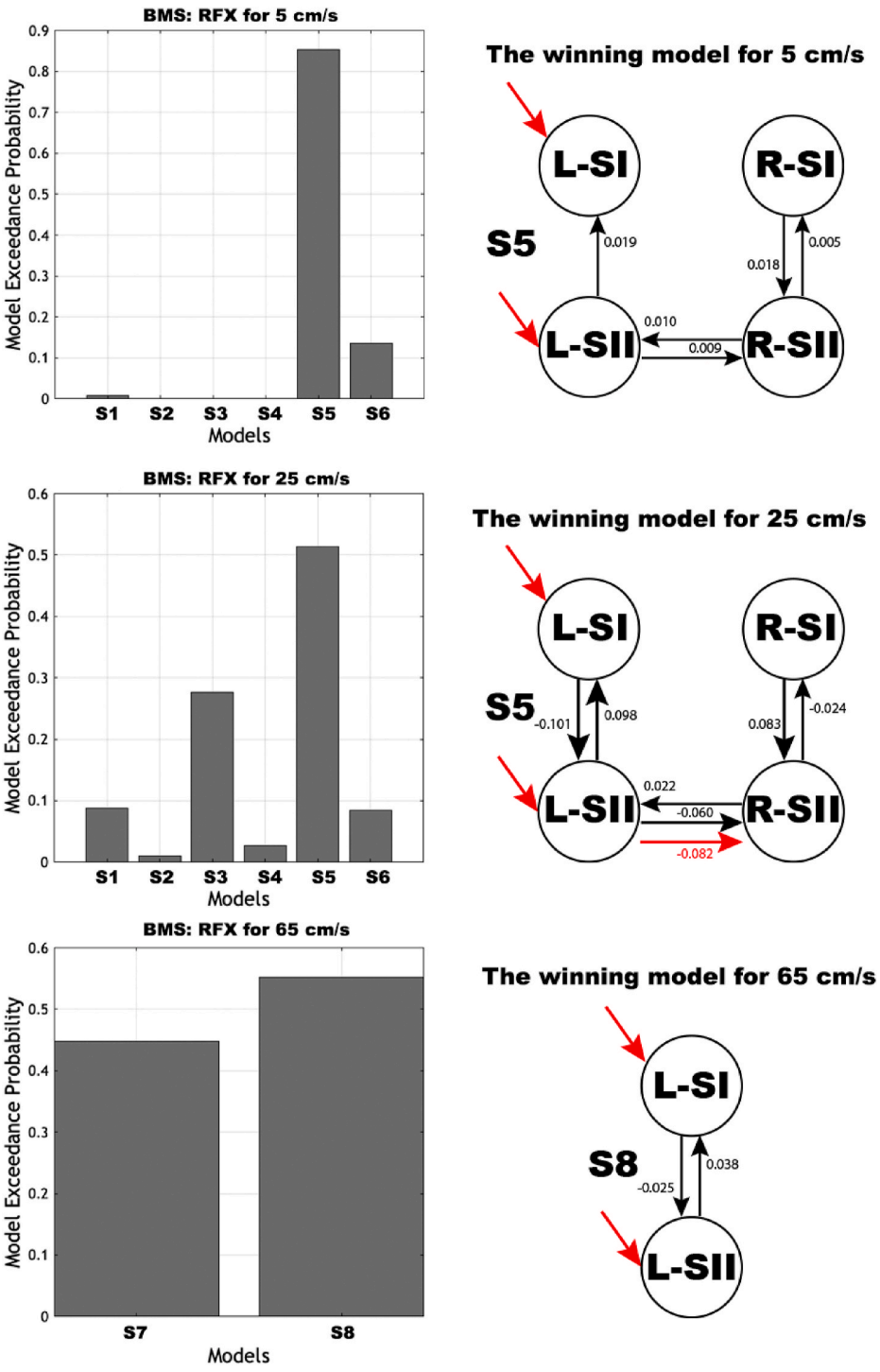

Fig. 5. BMS: RFX results for each velocity and the winning model for each velocity. The solid line indicates the probability that the posterior estimate of the parameter is not zero is more than 85%. L-SI: left primary somatosensory cortex, L-SII: left secondary somatosensory cortex, R–SI: right primary somatosensory cortex, R–SII: right secondary somatosensory cortex. Black arrows represent the intrinsic connections, Red arrows represent the modulatory connectivity and driving inputs to L-SI and L-SII. The line's thickness is determined by the connectivity parameter. (For interpretation of the references to colour in this figure legend, the reader is referred to the Web version of this article.)

3.3. Connectivity parameters of the winning models

3.3.1. Driving inputs and interhemispheric connections

BMA results of connectivity parameters for S5 and S8 models were shown in Table 2 and Fig. 5. Positive numbers indicate excitation, and negative numbers indicate inhibition. For all velocities, the driving inputs to the left SI and SII researched significance. There might be no significant difference between the modulation effect of 5 cm/s and the modulation effect of 25 cm/s on the forward ($p = 0.096$) connection from the left SII to the right SII.

3.3.2. Cross-modality plasticity and feedforward and feedback loops of cortico-cerebral networks

BMA results of connectivity parameters for S10, S11, S20, and S18 models were shown in Table 3 and Figs. 6 and 7. Positive numbers indicate excitation and negative numbers indicate inhibition. There might be no significant difference between the modulation effect of 5 cm/s and the modulation effect of 25 cm/s on forward connection ($p = 0.331$) from the left SI to the left M1 or forward connection ($p = 0.117$) from the left SII to the left M1. There might be no significant difference between the modulation effect of 5 cm/s and the modulation effect of 25 cm/s on the forward connections from the left SI to the left M1 ($p = 0.365$) and from the left SII to the left M1 ($p = 0.408$). In addition, there

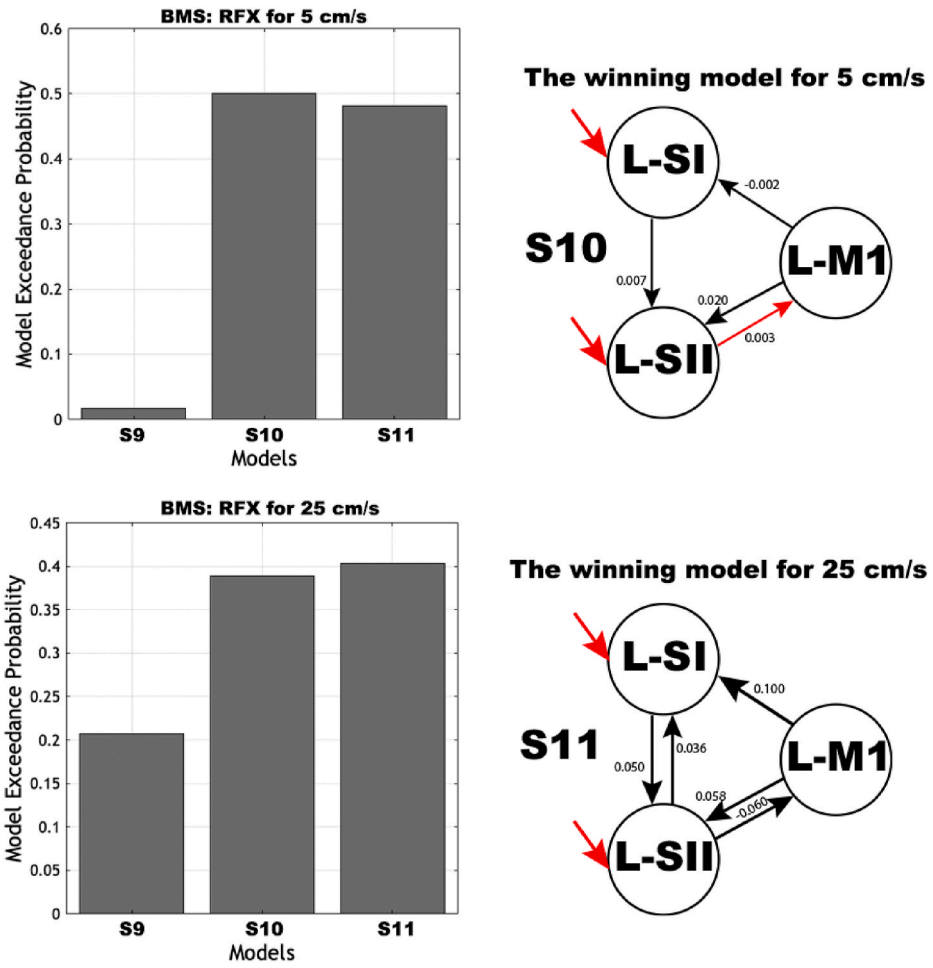

Fig. 6. BMS: RFX results for each velocity and the winning model for each velocity. The solid line indicates the probability that the posterior estimate of the parameter is not zero is more than 85%. L-SI: left primary somatosensory cortex, L-SII: left secondary somatosensory cortex, R–SI: right primary somatosensory cortex, R–SII: right secondary somatosensory cortex, L-M1: left primary motor cortex. Black arrows represent the intrinsic connections, Red arrows represent the modulatory connectivity and driving inputs to L-SI and L-SII. The line's thickness is determined by the connectivity parameter. (For interpretation of the references to colour in this figure legend, the reader is referred to the Web version of this article.)

might be no significant difference between the modulation effect of 5 cm/s and the modulation effect of 25 cm/s on the forward connections from the left SI to the right VI ($p = 0.788$), from the left SII to the right VI ($p = 0.219$), and from the left M1 to the right VI ($p = 0.573$), as well as the backward connections from the right VI to the left SI ($p = 0.189$), from the right VI to the left SII ($p = 0.177$), and the right VI to the left M1 ($p = 0.534$).

4. Discussion

The present study used DCM to examine how different velocity (5, 25, 65 cm/s) pneumotactile stimuli propagate among brain regions in the sensorimotor networks during passive saltatory pneumotactile stimuli on the right lower face, which has not been reported previously. First, the winning model S5 for 5 and 25 cm/s and S8 for 65 cm/s suggested both the contralateral left SI and SII directly received the driving inputs from the contralateral thalamus within the sensorimotor networks. In our model space, there were two possible ways for pneumotactile stimuli to enter the sensorimotor networks either through the left SI alone or through both the left SI and SII. Our results provided strong evidence that the cortical networks supporting higher-order processing of the facial pneumotactile stimuli (5 cm/s) involved parallel processing with driving inputs to both contralateral SI and SII. For medium and high velocities (25 and 65 cm/s), the most likely sources for the driving inputs were both left SI and SII, but the evidence was relatively weak. Second, model S5 provides direct evidence for the modulation effect on the forward interhemispheric connection from the contralateral left SII to the right SII, especially at the 25 cm/s pneumotactile stimuli. Third, the S10 and S11 models provided direct evidence that the velocity pneumotactile stimuli influenced the left M1 through the left SII alone for 5 cm/s. Our results indicate that passive pneumotactile stimulation may positively impact motor function through the left SII-M1 pathway. Furthermore, the S18 and S20 models provided direct evidence that the right cerebellar lobule VI plays a role in the sensorimotor network through intrinsic forward and backward neuronal pathways. But there were no significant modulation effects on the connections within the cortico-cerebellar network. All three-velocity pneumotactile stimuli did not elicit activation in the right cerebellar lobule VI in many participants. Thus, small sample sizes for model comparison among S12–S20 might contribute to the low power on detecting significance in modulation effects on the connections within the cortico-cerebellar network.

4.1. Parallel processing of velocity pneumotactile stimuli

In the present study, the right lower face was passively and non-invasively stimulated with air pressure pules from a spatial array of TAC-Cells (Wang et al., 2020). The pneumotactile stimuli are received through the cutaneous mechanoreceptors in the facial skin to the brainstem and then to the thalamus. Our DCM results provide strong evidence for a network able to parallel process of low velocity (5 cm/s) orofacial pneumotactile stimuli, which is in agreement with some studies (Klingner et al., 2015; Liang et al., 2011; Song et al., 2021) and also contrasts other findings (Disbrow et al., 2001; Kalberlah et al., 2013; Khoshnejad et al., 2014). Liang et al. has reported that non-nociceptive and nociceptive somatosensory inputs (electrical pulses to the right ankle that activate all subpopulation of fast-conducting myelinated Aβ fibers) are processed in parallel from the thalamus to

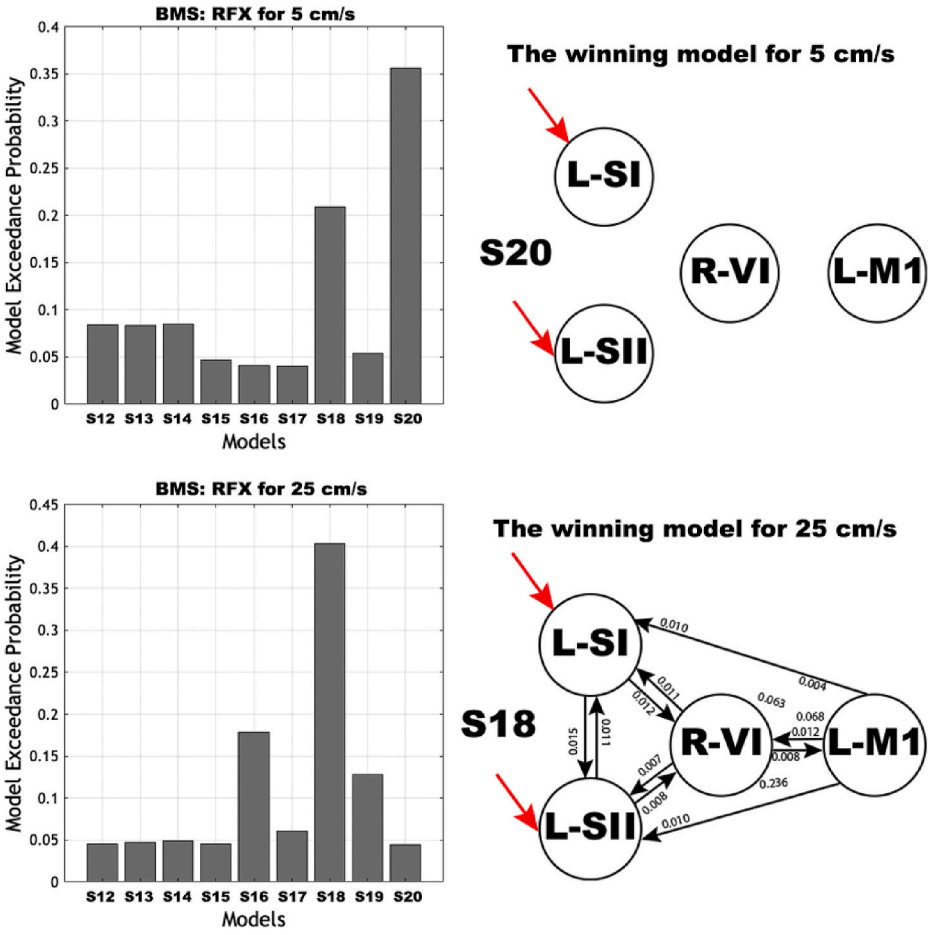

Fig. 7. BMS: RFX results for each velocity and the winning model for each velocity. The solid line indicates probability that the posterior estimate of the parameter is not zero is more than 85%. L-SI: left primary somatosensory cortex, L-SII: left secondary somatosensory cortex, R–SI: right primary somatosensory cortex, R–SII: right secondary somatosensory cortex, L-M1: left primary motor cortex, R–VI: right cerebellar lobule VI. Black arrows represent the intrinsic connections, Red arrows represent the modulatory connectivity and driving inputs to L-SI and L-SII. The line's thickness is determined by the connectivity parameter. (For interpretation of the references to colour in this figure legend, the reader is referred to the Web version of this article.)

Table 2
BMA results of connectivity parameters of S5 and S8.

Connections	Intrinsic strength 5 cm/s (Hz)	Effect of 5 cm/s (no unit)	Intrinsic strength 25 cm/s (Hz)	Effect of 25 cm/s (no unit)	Intrinsic strength 65 cm/s (Hz)
	S5 model		S5 model		S8 model
L-SI → L-SII	n.s.	n/a	−0.101†	n/a	−0.025†
L-SI ← L-SII	0.019†		0.098†		0.038†
L-SII → R–SII	0.009†	n.s.	−0.060†	−0.082†	n/a
L-SII ← R–SII	0.010†	n/a	0.022†	n/a	
R–SI → R–SII	0.018†	n/a	0.083†	n/a	
R–SI ← R–SII	0.005†		−0.024†		

Note: L-SI: left primary somatosensory cortex, L-SII: left secondary somatosensory cortex, R–SI: right primary somatosensory cortex, R–SII: right secondary somatosensory cortex, L-M1: left primary motor cortex. †Probability that the posterior estimate of the parameter is not zero is greater than 85%. n.s.: Probability that the posterior estimate of the parameter is not zero is equal or less than 85%. n/a: not applicable.

S1 and from the thalamus to S2 using DCM of fMRI data (Liang et al., 2011). Another MEG study (Klingner et al., 2015) used an electrical median nerve stimulus to the right wrist and found a parallel processing pathway to both contralateral SI and SII using DCM. A recent fMRI study (Song et al., 2021) used both nociceptive laser stimuli and electrical tactile stimuli to the right foot and identified parallel ascending pathways for both types of sensory stimuli through the thalamus to both SI and SII using DCM. The present study used pneumotactile stimuli to the right lower face area and found parallel processing of orofacial pneumotactile stimuli using DCM, which has not been reported previously. Contrary to our findings, two DCM studies supported serial processing from the contralateral SI to SII in response to innocuous and noxious electrical stimuli to the right sural nerve (Khoshnejad et al., 2014), as well as tactile vibratory stimuli to the left middle and index fingers (Kalberlah et al., 2013). The contradicting findings could result from various experimental settings (i.e., electrical versus tactile vibratory stimuli, stimulation to fingers/medial nerve versus foot/ankle). Additionally, the present study provides weak evidence in favor of parallel processing over serial processing of the orofacial pneumotactile stimuli for medium (25 cm/s) and high (65 cm/s) velocity. But there was significant intrinsic connectivity from the left SI to SII for 25 and 65 cm/s velocities. These findings from the present study suggested the coexistence of the parallel and serial processing theories regarding medium-to high-velocity pneumotactile processing, consistent with other studies (Chung et al., 2014; Cruccu et al., 2008). In summary, low velocity (5 cm/s) orofacial pneumotactile stimuli result in parallel processing, whereas medium (25 cm/s) and high (65 cm/s) velocities recruit both serial and parallel processing types in the present study.

4.2. Interhemispheric connection modulated by velocity pneumotactile stimuli

In this study, the S5 model optimally encoded the effect of velocity pneumotactile stimuli on a forward connection from the contralateral SII to the ipsilateral SII, suggesting interhemispheric modulation of effective connectivity in the SII due to the velocity pneumotactile stimuli to the lower face. Previous EEG and MEG studies have shown that

Table 3
BMA results of connectivity parameters of S10, S11, S18, and S20.

Connections	Intrinsic strength 5 cm/s	Effect of 5 cm/s	Intrinsic strength 25 cm/s	Effect of 25 cm/s	Intrinsic strength 5 cm/s	Effect of 5 cm/s	Intrinsic strength 25 cm/s	Effect of 25 cm/s
	S10 model		S11 model		S20 model		S18 model	
L-SI → L-SII	0.007†	n/a	0.050†	n/a	n.s.	n/a	0.015†	n/a
L-SI ← L-SII	n.s.		0.036†		n.s.		0.011†	
L-SI → L-M1	n.s.		n.s.	n.s.	n.s.	n.s.	n.s.	n.s.
L-SI ← L-M1	0.015†		0.100†	n/a	n.s.	n/a	0.010†	n/a
L-SII → L-M1	n.s.	0.003†	−0.060†	n.s.	n.s.	n.s.	n.s.	n.s.
L-SII ← L-M1	0.020†	n/a	0.058†	n/a	n.s.	n/a	0.010†	n/a
L-SI → R–VI	n/a				n.s.	n.s.	0.011†	n.s.
L-SI ← R–VI					n.s.	n.s.	0.012†	n.s.
L-SII → R–VI					n.s.	n.s.	0.008†	n/a
L-SII ← R–VI					n.s.	n.s.	0.007†	
L-M1 → R–VI					n.s.	n.s.	0.012†	n.s.
L-M1 ← R–VI					n.s.	n.s.	0.008†	n.s.

Note: L-SI: left primary somatosensory cortex, L-SII: left secondary somatosensory cortex, R–SI: right primary somatosensory cortex, R–SII: right secondary somatosensory cortex, L-M1: left primary motor cortex, R–VI: right cerebellar lobule VI. †Probability that the posterior estimate of the parameter is not zero is greater than 85%. n.s.: Probability that the posterior estimate of the parameter is not zero is equal or less than 85%. n/a: not applicable.

unilateral somatosensory stimuli activated bilateral SII, and the activation of the ipsilateral SII was delayed (Hoechstetter et al., 2001; Stancak et al., 2002). Our DCM results are consistent with previous work and suggest that the interhemispheric modulation effect from the contralateral SII to the ipsilateral SII might be related to bidirectional transcallosal connections linking both SII. Animal studies have found relatively dense transcallosal fibers connecting the contralateral SII and ipsilateral SII (Jones and Powell, 1969a; Pandya and Vignolo, 1968; Picard et al., 1990). Moreover, we identified an inhibitory connection for medium velocity (25 cm/s) stimuli but not for low velocity (5 cm/s) stimuli, which has not been reported previously. Compared to 5 cm/s, 25 cm/s has a higher temporal density of air-pulse stimulation and lower perception accuracy (Lamb, 1983). Thus, the medium velocity (25 cm/s) stimuli might be more affected by adaptation or repetition-suppressing process (Hollins et al., 1991; Popescu et al., 2013; Yang et al., 2014), whereas the 5-cm/s velocity stimuli might be processed as discrete stimuli instead of a constant motion across the skin (Depeault et al., 2013; Wacker et al., 2011). The medium velocity (25 cm/s) stimuli modulated the inhibitory forward connection from the contralateral SII to the ipsilateral SII, suggesting interhemispheric inhibition within SII for encoding medium velocity pneumotactile stimuli. Similarly, the interhemispheric inhibition within SII has been related to more complex bilateral receptive fields in SII than in SI for comparing spatial features of objects (Jung et al., 2012). For the high velocity (65 cm/s) stimuli, the interhemispheric modulation effect cannot be evaluated due to the lack of activation in the ipsilateral SII. This result is in agreement with our previous study (Wang et al., 2020) and suggested the high velocity exceeded the optimal range for moving tactile stimuli, which has been reported to be 3–25 cm/s for the face (Dreyer et al., 1979; Edin et al., 1995; Whitsel et al., 1986).

Our results also showed the significant intrinsic forward and backward connections between the contralateral left SII and ipsilateral right SII for 5 and 25 cm/s velocity stimuli. The average (baseline) effective connection between the left SII and right SII suggested the existence of interhemispheric connection within the sensorimotor network. The low velocity (5 cm/s) stimuli elicited excitatory connection from the contralateral SII to the ipsilateral SII, which aligns with other studies using either pressure or electrical stimulation (Chung et al., 2014; Khoshnejad et al., 2014). Khoshnejad et al. (2014) used electrical stimulation on the right sural nerve with low, moderate, and high-intensity levels and identified the excitatory connection from the contralateral SII to the ipsilateral SII for low (innocuous) and moderate (moderate-noxious) intensity levels but not for the high (high-noxious) intensity level. No participant in the present study reported discomfort or pain sensation. Therefore, pain-related neuronal networks may influence our results. However, the medium velocity (25 cm/s) stimuli elicited inhibitory connection from the contralateral SII to the ipsilateral SII. This result might be due to the complexity of the 25 cm/s velocity stimuli and effect from adaptation or repetition-suppressing process (Hollins et al., 1991; Popescu et al., 2013; Yang et al., 2014).

4.3. Cross-modality plasticity

Our DCM results provided weak evidence in favor of S10 over S11 for the low velocity (5 cm/s) and in favor of S11 over S10 for the medium velocity (25 cm/s). Nevertheless, both S10 and S11 indicated that the passive somatosensory inputs could modulate the primary motor cortex through either forward connection from the contralateral SII to the contralateral M1 (5 cm/s) or forward connections from both contralateral SI and SII to the contralateral M1 (25 cm/s). Therefore, our findings cannot definitely confirm which pathway passive somatosensory inputs influence the primary motor cortex. Still, our results support that the passive somatosensory inputs can affect motor function. The cross-modality plasticity theory suggested that somatosensory stimuli could evoke neural responses to promote motor learning (Ackerley et al., 2016; Ladda et al., 2014; Ludlow et al., 2008; Nasir et al., 2013; Sanes, 2003; Sanes and Donoghue, 2000; Veldman et al., 2018). Research has shown that the orofacial sensorimotor system is essential for sucking, swallowing, and speech production (Barlow, 1998; Barlow and Bradford, 1996; Barlow and Estep, 2006; Barlow et al., 2010; Barlow and Stumm, 2010; Sessle et al., 2005, 2007; Smith, 2016). Thus, our DCM results support that the passive pneumotactile stimulation could effectively modulate sensory and motor system to impact motor rehabilitation positively, in agreement with other studies (Ahn et al., 2016a; Chen et al., 2018a; Dinse and Tegenthoff, 2015; Heba et al., 2017; Macaluso et al., 2007). This is an important step for developing future early neurorehabilitation protocols. For instance, individuals cannot perform active movement rehabilitation tasks after severe brain injury (i.e., stroke, traumatic brain injury, etc.) and can benefit from passive sensory stimulation paradigms. Moreover, during the critical period when neural plasticity is the highest, if the passive tactile stimuli can be used to stimulate the sensory and motor system, it may improve the motor rehabilitation's outcomes later according to the cross-modality plasticity theory (Ackerley et al., 2016; Barlow et al., 2020; Blatow et al., 2011; Ladda et al., 2014; Ludlow et al., 2008; Nasir et al., 2013; Sanes, 2003; Sanes and Donoghue, 2000; Veldman et al., 2018). A recent EEG study has reported that passive unilateral somatosensory electrical stimulation can improve skill acquisition, consolidation, and interlimb transfer by increasing sensorimotor activity and connectivity (Veldman et al., 2018). Our noninvasive low velocity pulsed pneumotactile stimuli on the right lower face can modulate forward connection from the contralateral SII to the contralateral M1, supporting the cross-modality

plasticity theory. Further research is needed to provide strong evidence on our findings and uncover the neural mechanisms that drive motor rehabilitation through passive pneumotactile stimuli.

4.4. The role of right cerebellar lobule VI

The right cerebellar lobule VI has been suggested to be part of the sensorimotor somatotopic representations for the face (Grodd et al., 2001). In the present study, DCM results support that the right cerebellar lobule VI plays a role in the sensorimotor system during passive orofacial pneumotactile stimulation. Converging evidence from functional neuroimaging studies has shown that the cerebellum has multiple sensorimotor somatotopic representations (Bernard et al., 2013; Boillat et al., 2020; Bushara et al., 2001; Grodd et al., 2001; Kipping et al., 2013; Mottolese et al., 2013) and plays a critical role in motor functions (i.e., motor control, motor learning, etc.) and sensorimotor integration (Baumann et al., 2015; Buckner et al., 2011; Wolpert et al., 2011). Our DCM results revealed effective connectivity of the cortico-cerebral networks and suggested the involvements of both intrinsic forward (connections to the cerebellar) and backward (connections from the cerebellar) connections in cerebral-motor cortex connectivity. However, our DCM results were limited and might have type II errors due to significant individual differences in cerebellar activation patterns resulting in a small sample size. Similarly, the insignificance of connections involving the right cerebellar lobule VI within the neural networks can also be due to a small sample size. Thus, the role of the right cerebellar lobule VI may still need validity of future study with a large sample size. Only seven participants' time series from 5 cm/s stimuli and five participants' time series from 25 cm/s were successfully extracted and included in the DCM analyses. A recent study also reported that vibrotactile stimulation paradigms produced weaker activity in the cerebellum than the motor paradigms (Ashida et al., 2019). Resting-state functional MRI data has reported the functional connectivity between the right lobule VI and the left M1 (Kipping et al., 2013). Our DCM results provided direct evidence on both intrinsic forward and backward connections between the right lobule VI and the contralateral left SI and M1. However, the modulation effect from the tactile stimulation was not significant, which may be due to the small number of participants included in the cerebellum DCM analysis or weak activity in the cerebellum during passive tactile stimulation paradigms. Future studies with more participants are needed to elucidate the cortico-cerebellar network involved in sensory processing.

4.5. Limitations

This study has some limitations. First, we investigated effective connectivity on a dataset that has been described in our previous publications (Custead et al., 2017; Wang et al., 2020), which has limited the sample size to the original 20. Due to the individual variations in the functional spatial locations of pneumotactile velocity stimuli, the number of participants who have significant brain activity in the right SII and VI was small among all 20 participants. Therefore, the present study with a relatively small sample size may not have the statistical power to detect a small effect in the data (i.e., non-significant results in models S10, 11, 18, and 20), possibly resulting in a type II error. Second, the present study used DCM which is a hypothesis-driven approach for investigating the interactions among pre-defined ROIs. Model space and ROI are limited to what has been proposed in this study. There might be more models which could be defined for detecting effective connectivity among SI, SII, and M1. S10 and S11 in this study might belong to the same model family if we define more models in the model space. The stochastic DCM used in this study is not suitable for large-scale brain networks with many regions since stochastic DCM estimates both effective connectivity and hidden neuronal fluctuations that are computationally intensive and can only support a limited number of brain regions (Li et al., 2020; Razi et al., 2017). Lastly, the variational Bayesian methods used for DCM treat the posterior over parameters as Gaussian, which is not suitable for highly non-linear models. The bilinear DCM is sufficient for the present study because specifying the anatomical source of the modulatory processes is not relevant. Otherwise, nonlinear DCM can be utilized to allow the connection strength to depend on activity in remote neuronal populations (Friston et al., 2000, 2003, 2019; Stephan et al., 2008, 2010).

5. Conclusions

In summary, the present study examined effective connectivity evoked by the orofacial pneumotactile perception of velocity using DCM on 20 neurotypical adults' fMRI data, which has not been reported previously. Our DCM results demonstrated both similarities and differences in effective connectivity across the three-velocity orofacial pneumotactile stimulation. First, our DCM analyses suggested that the low velocity orofacial pneumotactile stimuli were processed in parallel through the contralateral SI and SII, and the medium and high-velocity stimuli recruited both serial and parallel processing types, supporting the coexistence of the parallel and serial processing theories during the passive orofacial pneumotactile stimulation paradigms. Second, the medium velocity orofacial pneumotactile stimuli modulated interhemispheric forward connections from the contralateral SII to the ipsilateral SII serially. Third, the significant modulation effect on forward connections between the contralateral SI and M1 during the low velocity orofacial pneumotactile stimulation supports the notion that the passive somatosensory inputs can affect the motor function. Therefore, the implication from our finding suggests that passive pneumotactile saltatory stimulation may bolster functional recovery during sensorimotor rehabilitation. Finally, we demonstrated that the right cerebellar lobule VI plays a role in the sensorimotor system. In the future, we can design sensorimotor rehabilitation protocols for stroke survivors using multichannel TAC-Cell arrays and fMRI or MEG, or both to evaluate the efficacy of the rehabilitation protocols.

Conflict of interest

All authors declare no competing interests.

Ethics approval statement

All procedures performed in studies involving human participants were in accordance with the ethical standards of the Institutional Review Board of University of Nebraska-Lincoln.

Data availability statement

The data that support the findings of this study are available on request from the corresponding author. The data are not publicly available due to privacy or ethical restrictions.

Funding statement

This work was supported by funds from the Barkley Trust (SB and YW), Nebraska Tobacco Settlement Biomedical Research Development, College of Education and Human Sciences, and the Office of Research and Economic Development.

Declaration of competing interest

The authors declare that they have no known competing financial interests or personal relationships that could have appeared to influence the work reported in this paper.

Acknowledgements

We thank our participants and undergraduate research assistants from the UNL UCARE program, courtesy of the Pepsi Quasi Endowment and Union Bank & Trust.

References

Ackerley, R., Borich, M., Oddo, C.M., Ionta, S., 2016. Insights and perspectives on sensory-motor integration and rehabilitation. Multisensory Res. 29, 607–633.
Ackerley, R., Hassan, E., Curran, A., Wessberg, J., Olausson, H., McGlone, F., 2012. An fMRI study on cortical responses during active self-touch and passive touch from others. Front. Behav. Neurosci. 6, 51.
Ahn, S.-N., Lee, J.-W., Hwang, S., 2016a. Tactile perception for stroke induce changes in electroencephalography. Hong Kong J. Occup. Ther. 28, 1–6.
Ahn, S.N., Lee, J.W., Hwang, S., 2016b. Tactile perception for stroke induce changes in electroencephalography. Hong Kong J. Occup. Ther. 28, 1–6.
Albus, J.S., 1971. A theory of cerebellar function. Math. Biosci. 10, 25–61.
Ashida, R., Cerminara, N.L., Edwards, R.J., Apps, R., Brooks, J.C.W., 2019. Sensorimotor, language, and working memory representation within the human cerebellum. Hum. Brain Mapp. 40, 4732–4747.
Bannister, L.C., Crewther, S.G., Gavrilescu, M., Carey, L.M., 2015. Improvement in touch sensation after stroke is associated with resting functional connectivity changes. Front. Neurol. 6, 165.
Barlow, S.M., 1998. Real time modulation of speech-orofacial motor performance by means of motion sense. J. Commun. Disord. 31, 511–534.
Barlow, S.M., Bradford, P.T., 1996. Comparison of perioral reflex modulation in the upper and lower lip. J. Speech Lang. Hear. Res. 39, 55–75.
Barlow, S.M., Custead, R., Lee, J., Hozan, M., Greenwood, J., 2020. Wireless sensing of lower lip and thumb-index finger 'ramp-and-hold' isometric force dynamics in a small cohort of unilateral MCA stroke: discussion of preliminary findings. Sensors 20.
Barlow, S.M., Estep, M., 2006. Central pattern generation and the motor infrastructure for suck, respiration, and speech. J. Commun. Disord. 39, 366–380.
Barlow, S.M., Lund, J.P., Estep, M., Kolta, A., 2010. Central pattern generators for orofacial movements and speech. In: Handbook of Mammalian Vocalization - an Integrative Neuroscience Approach, pp. 351–369.
Barlow, S.M., Stumm, S., 2010. Speech Production: Adult. Encyclopedia of Neuroscience. Elsevier Ltd, pp. 247–254.
Baumann, O., Borra, R.J., Bower, J.M., Cullen, K.E., Habas, C., Ivry, R.B., Leggio, M., Mattingley, J.B., Molinari, M., Moulton, E.A., Paulin, M.G., Pavlova, M.A., Schmahmann, J.D., Sokolov, A.A., 2015. Consensus paper: the role of the cerebellum in perceptual processes. Cerebellum 14, 197–220.
Benjamini, Y., Hochberg, Y., 1995. Controlling the false discovery rate: a practical and powerful approach to multiple testing. J. Roy. Stat. Soc. B 57, 289–300.
Bernard, J.A., Peltier, S.J., Wiggins, J.L., Jaeggi, S.M., Buschkuehl, M., Fling, B.W., Kwak, Y., Jonides, J., Monk, C.S., Seidler, R.D., 2013. Disrupted cortico-cerebellar connectivity in older adults. Neuroimage 83, 103–119.
Blatow, M., Reinhardt, J., Riffel, K., Nennig, E., Wengenroth, M., Stippich, C., 2011. Clinical functional MRI of sensorimotor cortex using passive motor and sensory stimulation at 3 Tesla. J. Magn. Reson. Imag. 34, 429–437.
Boillat, Y., Bazin, P.L., van der Zwaag, W., 2020. Whole-body somatotopic maps in the cerebellum revealed with 7T fMRI. Neuroimage 211, 116624.
Buckner, R.L., 2013. The cerebellum and cognitive function: 25 years of insight from anatomy and neuroimaging. Neuron 80, 807–815.
Buckner, R.L., Krienen, F.M., Castellanos, A., Diaz, J.C., Yeo, B.T., 2011. The organization of the human cerebellum estimated by intrinsic functional connectivity. J. Neurophysiol. 106, 2322–2345.
Burton, H., Carlson, M., 1986. Second somatic sensory cortical area (SII) in a prosimian primate, Galago crassicaudatus. J. Comp. Neurol. 247, 200–220.
Bushara, K.O., Wheat, J.M., Khan, A., Mock, B.J., Turski, P.A., Sorenson, J., Brooks, B.R., 2001. Multiple tactile maps in the human cerebellum. Neuroreport 12, 2483–2486.
Carter, A.R., Astafiev, S.V., Lang, C.E., Connor, L.T., Rengachary, J., Strube, M.J., Pope, D.L., Shulman, G.L., Corbetta, M., 2010. Resting interhemispheric functional magnetic resonance imaging connectivity predicts performance after stroke. Ann. Neurol. 67, 365–375.
Chen, X., Liu, F., Yan, Z., Cheng, S., Liu, X., Li, H., Li, Z., 2018a. Therapeutic effects of sensory input training on motor function rehabilitation after stroke. Medicine 97.
Chen, X., Liu, F., Yan, Z., Cheng, S., Liu, X., Li, H., Li, Z., 2018b. Therapeutic effects of sensory input training on motor function rehabilitation after stroke. Medicine (Baltim.) 97, e13387.
Chung, Y.G., Han, S.W., Kim, H.-S., Chung, S.-C., Park, J.-Y., Wallraven, C., Kim, S.-P., 2014. Intra-and inter-hemispheric effective connectivity in the human somatosensory cortex during pressure stimulation. BMC Neurosci. 15, 1–10.
Compston, A., 2011. Brain. Editorial. Brain 134, 1251–1253.
Conforto, A.B., Cohen, L.G., dos Santos, R.L., Scaff, M., Marie, S.K., 2007. Effects of somatosensory stimulation on motor function in chronic cortico-subcortical strokes. J. Neurol. 254, 333–339.
Cramer, S.C., Crafton, K.R., 2006. Somatotopy and movement representation sites following cortical stroke. Exp. Brain Res. 168, 25–32.
Cruccu, G., Aminoff, M., Curio, G., Guerit, J., Kakigi, R., Mauguiere, F., Rossini, P., Treede, R.-D., Garcia-Larrea, L., 2008. Recommendations for the clinical use of somatosensory-evoked potentials. Clin. Neurophysiol. 119, 1705–1719.
Custead, R., Oh, H., Wang, Y., Barlow, M.S., 2017. Brain encoding of saltatory velocity through a pulsed pneumotactile array in the lower face. Brain Res. 1677, 58–73.
D'Angelo, E., Casali, S., 2012. Seeking a unified framework for cerebellar function and dysfunction: from circuit operations to cognition. Front. Neural Circ. 6, 116.
Depeault, A., Meftah el, M., Chapman, C.E., 2013. Neuronal correlates of tactile speed in primary somatosensory cortex. J. Neurophysiol. 110, 1554–1566.
Dinse, H.R., Tegenthoff, M., 2015. Evoking plasticity through sensory stimulation: implications for learning and rehabilitation. e-Neuroforum 6, 11–20.
Disbrow, E., Roberts, T., Poeppel, D., Krubitzer, L., 2001. Evidence for interhemispheric processing of inputs from the hands in human S2 and PV. J. Neurophysiol. 85, 2236–2244.
Dreyer, D.A., Duncan, G.H., Wong, C.L., Whitsel, B.L., 1979. Factors influencing capacity to judge direction of tactile stimulus movement on the face. J. Dent. Res. 58, 2052–2057.
Dum, R.P., Strick, P.L., 2003. An unfolded map of the cerebellar dentate nucleus and its projections to the cerebral cortex. J. Neurophysiol. 89, 634–639.
Edin, B.B., Essick, G.K., Trulsson, M., Olsson, K.A., 1995. Receptor encoding of moving tactile stimuli in humans. I. Temporal pattern of discharge of individual low-threshold mechanoreceptors. J. Neurosci. 15, 830–847.
Fabri, M., Polonara, G., Quattrini, A., Salvolini, U., Del Pesce, M., Manzoni, T., 1999. Role of the corpus callosum in the somatosensory activation of the ipsilateral cerebral cortex: an fMRI study of callosotomized patients. Eur. J. Neurosci. 11, 3983–3994.
Forss, N., Salmelin, R., Hari, R., 1994. Comparison of somatosensory evoked fields to airpuff and electric stimuli. Electroencephalogr. Clin. Neurophysiology Evoked Potentials Sect. 92, 510–517.
Francis, S., Kelly, E., Bowtell, R., Dunseath, W., Folger, S., McGlone, F., 2000. fMRI of the responses to vibratory stimulation of digit tips. Neuroimage 11, 188–202.
Friedman, D., Jones, E., Burton, H., 1980. Representation pattern in the second somatic sensory area of the monkey cerebral cortex. J. Comp. Neurol. 192, 21–41.
Friston, K., Moran, R., Seth, A.K., 2013. Analysing connectivity with Granger causality and dynamic causal modelling. Curr. Opin. Neurobiol. 23, 172–178.
Friston, K.J., 2011. Functional and effective connectivity: a review. Brain Connect. 1, 13–36.
Friston, K.J., Harrison, L., Penny, W., 2003. Dynamic causal modelling. Neuroimage 19, 1273–1302.
Friston, K.J., Mechelli, A., Turner, R., Price, C.J., 2000. Nonlinear responses in fMRI: the Balloon model, Volterra kernels, and other hemodynamics. Neuroimage 12, 466–477.
Friston, K.J., Preller, K.H., Mathys, C., Cagnan, H., Heinzle, J., Razi, A., Zeidman, P., 2019. Dynamic causal modelling revisited. Neuroimage 199, 730–744.
Grodd, W., Hulsmann, E., Lotze, M., Wildgruber, D., Erb, M., 2001. Sensorimotor mapping of the human cerebellum: fMRI evidence of somatotopic organization. Hum. Brain Mapp. 13, 55–73.
Hari, R., Karhu, J., Hämäläinen, M., Knuutila, J., Salonen, O., Sams, M., Vilkman, V., 1993. Functional organization of the human first and second somatosensory cortices: a neuromagnetic study. Eur. J. Neurosci. 5, 724–734.
Heba, S., Lenz, M., Kalisch, T., Hoffken, O., Schweizer, L.M., Glaubitz, B., Puts, N.A.J., Tegenthoff, M., Dinse, H.R., Schmidt-Wilcke, T., 2017. Regionally specific regulation of sensorimotor network connectivity following tactile improvement. Neural Plast. 2017, 5270532.
Hoechstetter, K., Rupp, A., Stančák, A., Meinck, H.-M., Stippich, C., Berg, P., Scherg, M., 2001. Interaction of tactile input in the human primary and secondary somatosensory cortex—a magnetoencephalographic study. Neuroimage 14, 759–767.
Hollins, M., Delemos, K.A., Goble, A.K., 1991. Vibrotactile adaptation on the face. Percept. Psychophys. 49, 21–30.
Ionta, S., Martuzzi, R., Salomon, R., Blanke, O., 2014. The brain network reflecting bodily self-consciousness: a functional connectivity study. Soc. Cognit. Affect Neurosci. 9, 1904–1913.
Jones, E., 1998. The core and matrix of thalamic organization. Neuroscience 85, 331–345.
Jones, E., Powell, T., 1969a. Connexions of the somatic sensory cortex of the rhesus monkey: I.—ipsilateral cortical connexions. Brain 92, 477–502.
Jones, E., Powell, T., 1969b. Connexions of the somatic sensory cortex of the rhesus monkey: II.—contralateral cortical connexions. Brain 92, 717–730.
Jung, P., Klein, J.C., Wibral, M., Hoechstetter, K., Bliem, B., Lu, M.-K., Wahl, M., Ziemann, U., 2012. Spatiotemporal dynamics of bimanual integration in human somatosensory cortex and their relevance to bimanual object manipulation. J. Neurosci. 32, 5667–5677.
Kalberlah, C., Villringer, A., Pleger, B., 2013. Dynamic causal modeling suggests serial processing of tactile vibratory stimuli in the human somatosensory cortex—an fMRI study. Neuroimage 74, 164–171.
Kass, R.E., Raftery, A.E., 1995. Bayes factors. J. Am. Stat. Assoc. 90, 773–795.
Khoshnejad, M., Piché, M., Saleh, S., Duncan, G., Rainville, P., 2014. Serial processing in primary and secondary somatosensory cortex: a DCM analysis of human fMRI data in response to innocuous and noxious electrical stimulation. Neurosci. Lett. 577, 83–88.
Kipping, J.A., Grodd, W., Kumar, V., Taubert, M., Villringer, A., Margulies, D.S., 2013. Overlapping and parallel cerebello-cerebral networks contributing to sensorimotor control: an intrinsic functional connectivity study. Neuroimage 83, 837–848.
Klingner, C.M., Brodoehl, S., Huonker, R., Götz, T., Baumann, L., Witte, O.W., 2015. Parallel processing of somatosensory information: evidence from dynamic causal modeling of MEG data. Neuroimage 118, 193–198.
Krubitzer, L.A., Kaas, J.H., 1992. The somatosensory thalamus of monkeys: cortical connections and a redefinition of nuclei in marmosets. J. Comp. Neurol. 319, 123–140.

Ladda, A.M., Pfannmoeller, J.P., Kalisch, T., Roschka, S., Platz, T., Dinse, H.R., Lotze, M., 2014. Effects of combining 2 weeks of passive sensory stimulation with active hand motor training in healthy adults. PLoS One 9, e84402.
Lamb, G.D., 1983. Tactile discrimination of textured surfaces: psychophysical performance measurements in humans. J. Physiol. 338, 551–565.
Li, G., Liu, Y., Zheng, Y., Li, D., Liang, X., Chen, Y., Cui, Y., Yap, P.T., Qiu, S., Zhang, H., Shen, D., 2020. Large-scale dynamic causal modeling of major depressive disorder based on resting-state functional magnetic resonance imaging. Hum. Brain Mapp. 41, 865–881.
Liang, M., Mouraux, A., Iannetti, G.D., 2011. Parallel processing of nociceptive and non-nociceptive somatosensory information in the human primary and secondary somatosensory cortices: evidence from dynamic causal modeling of functional magnetic resonance imaging data. J. Neurosci. 31, 8976–8985.
Lin, Y.Y., Kajola, M., 2003. Neuromagnetic somatosensory responses to natural moving tactile stimulation. Can. J. Neurol. Sci. 30, 31–35.
Ludlow, C.L., Hoit, J., Kent, R., Ramig, L.O., Shrivastav, R., Strand, E., Yorkston, K., Sapienza, C.M., 2008. Translating Principles of Neural Plasticity into Research on Speech Motor Control Recovery and Rehabilitation.
Lundblad, L.C., Olausson, H.W., Hermansson, A.K., Wasling, H.B., 2011. Cortical processing of tactile direction discrimination based on spatiotemporal cues in man. Neurosci. Lett. 501, 45–49.
Macaluso, E., Cherubini, A., Sabatini, U., 2007. Bimanual passive movement: functional activation and inter-regional coupling. Front. Integr. Neurosci. 1, 5.
Marr, D., 1969. A theory of cerebellar cortex. J Physiol 202, 437–470.
Mohajerani, M.H., Aminoltejari, K., Murphy, T.H., 2011. Targeted mini-strokes produce changes in interhemispheric sensory signal processing that are indicative of disinhibition within minutes. Proc. Natl. Acad. Sci. U. S. A. 108, E183–E191.
Mottolese, C., Richard, N., Harquel, S., Szathmari, A., Sirigu, A., Desmurget, M., 2013. Mapping motor representations in the human cerebellum. Brain 136, 330–342.
Murase, N., Duque, J., Mazzocchio, R., Cohen, L.G., 2004. Influence of interhemispheric interactions on motor function in chronic stroke. Ann. Neurol. 55, 400–409.
Nasir, S.M., Darainy, M., Ostry, D.J., 2013. Sensorimotor adaptation changes the neural coding of somatosensory stimuli. J. Neurophysiol. 109, 2077–2085.
Norrsell, U., Olausson, H., 1994. Spatial cues serving the tactile directional sensibility of the human forearm. J Physiol 478 Pt 3, 533–540.
Oh, H., Custead, R., Wang, Y., Barlow, M.S., 2017. Neural encoding of saltatory pneumotactile velocity in human glabrous hand. PLoS One 12, e0183532.
Pandya, D.N., Vignolo, L.A., 1968. Interhemispheric neocortial projections of somatosensory areas I and II in the rhesus monkey. Brain Res. 7, 300–303.
Pearson, K., 2000. Motor systems. Curr. Opin. Neurobiol. 10, 649–654.
Pellegrino, G., Tomasevic, L., Tombini, M., Assenza, G., Bravi, M., Sterzi, S., Giacobbe, V., Zollo, L., Guglielmelli, E., Cavallo, G., Vernieri, F., Tecchio, F., 2012. Inter-hemispheric coupling changes associate with motor improvements after robotic stroke rehabilitation. Restor. Neurol. Neurosci. 30, 497–510.
Picard, N., Lepore, F., Ptito, M., Guillemot, J.-P., 1990. Bilateral interaction in the second somatosensory area (SII) of the cat and contribution of the corpus callosum. Brain Res. 536, 97–104.
Pons, T., Kaas, J., 1986. Corticocortical connections of area 2 of somatosensory cortex in macaque monkeys: a correlative anatomical and electrophysiological study. J. Comp. Neurol. 248, 313–335.
Popescu, E.A., Barlow, S.M., Venkatesan, L., Wang, J., Popescu, M., 2013. Adaptive changes in the neuromagnetic response of the primary and association somatosensory areas following repetitive tactile hand stimulation in humans. Hum. Brain Mapp. 34, 1415–1426.
Powell, J., Pandyan, A.D., Granat, M., Cameron, M., Stott, D.J., 1999. Electrical stimulation of wrist extensors in poststroke hemiplegia. Stroke 30, 1384–1389.
Raij, T., Karhu, J., Kicic, D., Lioumis, P., Julkunen, P., Lin, F.H., Ahveninen, J., Ilmoniemi, R.J., Makela, J.P., Hamalainen, M., Rosen, B.R., Belliveau, J.W., 2008. Parallel input makes the brain run faster. Neuroimage 40, 1792–1797.
Razi, A., Seghier, M.L., Zhou, Y., McColgan, P., Zeidman, P., Park, H.J., Sporns, O., Rees, G., Friston, K.J., 2017. Large-scale DCMs for resting-state fMRI. Netw Neurosci 1, 222–241.
Rosa, M., Friston, K., Penny, W., 2012. Post-hoc selection of dynamic causal models. J. Neurosci. Methods 208, 66–78.
Rowe, M.J., Turman, A.B., Murray, G.M., Zhang, H.Q., 1996. Parallel organization of somatosensory cortical areas I and II for tactile processing. Clin. Exp. Pharmacol. Physiol. 23, 931–938.
Ruben, J., Schwiemann, J., Deuchert, M., Meyer, R., Krause, T., Curio, G., Villringer, K., Kurth, R., Villringer, A., 2001. Somatotopic organization of human secondary somatosensory cortex. Cerebr. Cortex 11, 463–473.
Sanes, J., 2003. Neocortical mechanisms in motor learning. Curr. Opin. Neurobiol. 13, 225–231.
Sanes, J., Donoghue, J.P., 2000. Plasticity and primary motor cortex. Annu. Rev. Neurosci. 23, 393–415.
Schmahmann, J.D., Caplan, D., 2006. Cognition, emotion and the cerebellum. Brain 129, 290–292.
Sessle, B., Adachi, K., Avivi-Arber, L., Lee, J., Nishiura, H., Yao, D., Yoshino, K., 2007. Neuroplasticity of face primary motor cortex control of orofacial movements. Arch. Oral Biol. 52, 334–337.
Sessle, B., Yao, D., Nishiura, H., Yoshino, K., Lee, J.C., Martin, R.E., Murray, G.M., 2005. Properties and plasticity of the primate somatosensory and motor cortex related to orofacial sensorimotor function. Clin. Exp. Pharmacol. Physiol. 32, 109–114.
Smith, A., 2016. The control of orofacial movements in speech. Crit. Rev. Oral Biol. Med. 3, 233–267.
Smith, P.S., Dinse, H.R., Kalisch, T., Johnson, M., Walker-Batson, D., 2009. Effects of repetitive electrical stimulation to treat sensory loss in persons poststroke. Arch. Phys. Med. Rehabil. 90, 2108–2111.
Smith, S.M., Miller, K.L., Salimi-Khorshidi, G., Webster, M., Beckmann, C.F., Nichols, T. E., Ramsey, J.D., Woolrich, M.W., 2011. Network modelling methods for FMRI. Neuroimage 54, 875–891.
Song, Y., Su, Q., Yang, Q., Zhao, R., Yin, G., Qin, W., Iannetti, G.D., Yu, C., Liang, M., 2021. Feedforward and feedback pathways of nociceptive and tactile processing in human somatosensory system: a study of dynamic causal modeling of fMRI data. Neuroimage 234, 117957.
Stancak, A., Hoechstetter, K., Tintera, J., Vrana, J., Rachmanova, R., Kralik, J., Scherg, M., 2002. Source activity in the human secondary somatosensory cortex depends on the size of corpus callosum. Brain Res. 936, 47–57.
Stephan, K.E., Kasper, L., Harrison, L.M., Daunizeau, J., den Ouden, H.E., Breakspear, M., Friston, K.J., 2008. Nonlinear dynamic causal models for fMRI. Neuroimage 42, 649–662.
Stephan, K.E., Penny, W.D., Moran, R.J., den Ouden, H.E., Daunizeau, J., Friston, K.J., 2010. Ten simple rules for dynamic causal modeling. Neuroimage 49, 3099–3109.
Stephan, K.E., Weiskopf, N., Drysdale, P.M., Robinson, P.A., Friston, K.J., 2007. Comparing hemodynamic models with DCM. Neuroimage 38, 387–401.
Tellmann, S., Bludau, S., Eickhoff, S., Mohlberg, H., Minnerop, M., Amunts, K., 2015. Cytoarchitectonic mapping of the human brain cerebellar nuclei in stereotaxic space and delineation of their co-activation patterns. Front. Neuroanat. 9, 54.
Thurling, M., Kuper, M., Stefanescu, R., Maderwald, S., Gizewski, E.R., Ladd, M.E., Timmann, D., 2011. Activation of the dentate nucleus in a verb generation task: a 7T MRI study. Neuroimage 57, 1184–1191.
Turman, A.B., Ferrington, D.G., Ghosh, S., Morley, J.W., Rowe, M.J., 1992. Parallel processing of tactile information in the cerebral cortex of the cat: effect of reversible inactivation of SI on responsiveness of SII neurons. J. Neurophysiol. 67, 411–429.
Veldman, M.P., Maurits, N.M., Zijdewind, I., Maffiuletti, N.A., van Middelkoop, S., Mizelle, J.C., Hortobágyi, T., 2018. Somatosensory electrical stimulation improves skill acquisition, consolidation, and transfer by increasing sensorimotor activity and connectivity. J. Neurophysiol. 120, 281–290.
Wacker, E., Spitzer, B., Lutzkendorf, R., Bernarding, J., Blankenburg, F., 2011. Tactile motion and pattern processing assessed with high-field FMRI. PLoS One 6, e24860.
Wang, Y., Sibaii, F., Custead, R., Oh, H., Barlow, S.M., 2020. Functional connectivity evoked by orofacial tactile perception of velocity. Front. Neurosci. 14.
Whitsel, B.L., Franzen, O., Dreyer, D.A., Hollins, M., Young, M., Essick, G.K., Wong, C., 1986. Dependence of subjective traverse length on velocity of moving tactile stimuli. Somatosens. Res. 3, 185–196.
Witter, L., De Zeeuw, C.I., 2015. Regional functionality of the cerebellum. Curr. Opin. Neurobiol. 33, 150–155.
Wolpert, D.M., Diedrichsen, J., Flanagan, J.R., 2011. Principles of sensorimotor learning. Nat. Rev. Neurosci. 12, 739–751.
Yang, J., Yu, Y., Kunita, A., Huang, Q., Wu, J., Sawamoto, N., Fukuyama, H., 2014. Tactile priming modulates the activation of the fronto-parietal circuit during tactile angle match and non-match processing: an fMRI study. Front. Hum. Neurosci. 8, 926.
Zeidman, P., Jafarian, A., Corbin, N., Seghier, M.L., Razi, A., Price, C.J., Friston, K.J., 2019a. A guide to group effective connectivity analysis, part 1: first level analysis with DCM for fMRI. Neuroimage 200, 174–190.
Zeidman, P., Jafarian, A., Seghier, M.L., Litvak, V., Cagnan, H., Price, C.J., Friston, K.J., 2019b. A guide to group effective connectivity analysis, part 2: second level analysis with PEB. Neuroimage 200, 12–25.
Zhang, H.Q., Murray, G.M., Coleman, G.T., Turman, A.B., Zhang, S.P., Rowe, M.J., 2001. Functional characteristics of the parallel SI-and SII-projecting neurons of the thalamic ventral posterior nucleus in the marmoset. J. Neurophysiol. 85, 1805–1822.
Zhang, H.Q., Murray, G.M., Turman, A.B., Mackie, P.D., Coleman, G.T., Rowe, M.J., 1996. Parallel processing in cerebral cortex of the marmoset monkey: effect of reversible SI inactivation on tactile responses in SII. J. Neurophysiol. 76, 3633–3655.